International Journal of Heat and Fluid Flow 117 (2026) 110015

Contents lists available at ScienceDirect

International Journal of Heat and Fluid Flow

journal homepage: www.elsevier.com/locate/ijhff

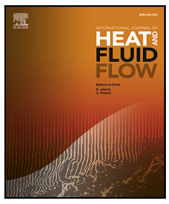

Direct Numerical Simulations of turbulent channel flow roughened with 2D triangular bars: On the Effective Distribution parametrization

Federica Bruno [a], Mauro De Marchis [b,*], Stefano Leonardi [c]

[a] Department of Engineering and Architecture, University of Enna "Kore", Enna, Italy
[b] Department of Engineering, University of Palermo, Palermo, Italy
[c] Department of Mechanical Engineering, University of Texas at Dallas, Richardson, TX, USA

ARTICLE INFO

Keywords:
Roughness
Effective slope
DNS
Effective distribution

ABSTRACT

Turbulent flows over rough surfaces are a common phenomenon in engineering applications, yet predicting how the roughness affects the turbulent flow remains a challenge. In the present paper, we expand the results of Bruno et al. (2024) on the new geometrical parameter, the Effective Distribution (ED). Specifically, the effect of roughness on turbulent intensities has been investigated. The ED demonstrates improved correlations with both drag and roughness function across a wide range of surface configurations, including irregular rough surfaces generated by random sinusoidal functions. A detailed analysis of the ED equation reveals that the contributions of higher pinnacles and the spacing between roughness elements, play a dominant role in capturing the impact of roughness on drag and turbulent intensities. To investigate this issue, a detailed analysis of turbulent intensities modification induced by the roughness is performed, thus showing the highest pinnacle's role. These results emphasize the importance of considering these terms in the parametrization of rough surfaces.

1. Introduction

Rough surfaces are a fundamental feature in many engineering and environmental systems influencing turbulent flow behavior. Examples include the atmospheric boundary layer over urban areas (Oke (1988), Jiménez (2004)), the erosion of turbine blades (Bons (2005)), flow through heat exchangers and natural terrains with vegetation. The interaction between turbulent flows and surface roughness leads to increased drag, energy losses, and higher operational costs, making prediction and control of roughness-induced effects a critical design challenge across disciplines. Research on the influence of surface roughness dates back to the work of Nikuradse (1933), who studied flows over sand-grain roughness. Since then, extensive efforts have been devoted to understanding the complex interplay between roughness geometry and turbulence. One of the key developments in this area has been the roughness function, ΔU^+, introduced by Hama (1954), which quantifies the downward shift in the mean velocity profile caused by rough surfaces. Hereafter, the superscript $^+$ denotes variables made non-dimensional with inner variables $u_\tau = (\sqrt{\tau_s/\rho})$ and ν/u_τ, where u_τ is the friction velocity, ρ is the fluid density, ν is the kinematic viscosity, and τ_s is the wall shear stress, equal to the sum of the viscous (or skin frictional) stress $\overline{C_f} = \frac{1}{L_x}\int_0^{L_x}(\mu\partial\langle U^*\rangle/\partial y^*)(1/\rho U_c^2)ds$ and the form drag $\overline{P_d} = \frac{1}{L_x}\int_0^{L_x}\langle P\rangle\vec{n}\cdot\vec{x}ds$, ($\vec{n}$ is the normal to the surface, $\vec{x}$ is the unit vector in the streamwise direction, and s is a coordinate along the surface). The symbol $\langle\cdot\rangle$ indicates quantities averaged in the spanwise direction and time, * indicates dimensional units, L_x represents the streamwise length and μ is the dynamic viscosity. The downward shift ΔU^+ is often correlated with the equivalent sand grain roughness, k_s, as first proposed by Schlichting (1937). Hama's formulation for the roughness function is given by:

$$\Delta U^+ = \frac{1}{\kappa}\ln(k_s^+) + B \tag{1}$$

where κ is the von Kármán constant, $k_s^+ = k_s \cdot u_\tau/\nu$ is the non-dimensional roughness height, and B is a constant. However, as pointed out by several authors (see, among others, Flack et al. (2020)), k_s is not a direct geometrical measure of surface roughness and must be determined empirically, which limits its general applicability. In recent decades, researchers have introduced a variety of geometrical parameters to better characterize roughness effects. These include the mean roughness height, peak-to-valley distance, roughness density, skewness, kurtosis, and the Effective Slope (ES) (Sigal and Danberg (1990); Waigh and Kind (1998); Van Rij et al. (2002); Bons (2005); Flack and Schultz (2010); Chan et al. (2015); De Marchis et al. (2017); Busse et al. (2017); Forooghi et al. (2017); Thakkar et al. (2017); Piomelli (2019);

* Corresponding author.
E-mail address: mauro.demarchis@unipa.it (M. De Marchis).

https://doi.org/10.1016/j.ijheatfluidflow.2025.110015
Received 5 February 2025; Received in revised form 23 June 2025; Accepted 12 August 2025

De Marchis et al. (2020); Chung et al. (2021); Bruno et al. (2024a)). Despite these advancements, no single parameter has yet emerged as universally applicable, specifically for surfaces with irregular or complex geometries. This highlights the need for a more comprehensive approach to predict roughness effects on turbulence. Based on the findings of Bruno et al. (2024b), this study extends the analysis of the recently introduced Effective Distribution (ED) parameter. The ED incorporates multiple aspects of roughness geometry, including sheltering effects, peak interactions, and surface patterns. Although previous work demonstrated strong correlations between ED, drag and the roughness function for 2D triangular roughness and irregular surfaces, generated through random sinusoidal functions, the present study investigates the individual components of the ED and their contributions to the overall parametrization of roughness, better explaining the role of each quantity. Furthermore, to give more insights on the physics of a single roughness element, an in-depth analysis of the turbulent intensity components has been performed, focusing particularly on the contribution of roughness peaks to the production of rms values. By providing a more detailed understanding of the ED parameter and its correlation with drag and the roughness function, this study aims to advance our ability to predict the effects of surface roughness in practical applications. The paper is organized as follows: Section 2 describes the numerical methods used for Direct Numerical Simulations (DNS), Section 3 details the flow configurations analyzed, Section 4 presents the key findings and Section 5 summarizes the conclusions and outlines directions for future research.

2. Numerical procedure

In order to investigate the effect of 2D roughness elements transversally placed in the flow direction, several Direct Numerical Simulations were conducted in fully developed turbulent channel flows. The flow domain is bounded by an upper flat wall and a rough bottom wall. The non-dimensional Navier–Stokes and continuity equations for incompressible and neutrally stable flows are resolved, as follow:

$$\frac{\partial U_i}{\partial t} + \frac{\partial U_i U_j}{\partial x_j} = -\frac{\partial P}{\partial x_i} + \frac{1}{Re}\frac{\partial^2 U_i}{\partial x_j^2} + \Pi\delta_{i1}, \tag{2}$$

$$\nabla \cdot \boldsymbol{U} = 0, \tag{3}$$

where Re represents the Reynolds number based on the bulk velocity ($U_b = \frac{1}{h}\int_0^h U, dy$), which is kept constant over time, h denotes the channel's half-height, δ_{ij} is the Kronecker delta, U_i corresponds to the ith velocity component, x_i refers to the ith spatial coordinate, and P is the pressure. The simulations were performed to ensure a constant flow rate. In order to do this, a time-dependent pressure gradient Π is imposed at each iteration to balance friction and pressure drag. The Navier–Stokes equations were discretized in an orthogonal coordinate system using a staggered second-order central finite difference scheme. According to Orlandi and Leonardi (2006) a modified version of the immersed boundary method is applied to perform computations on complex geometries without requiring highly detailed body-fitted grids. This approach involves enforcing the condition $U_i = 0$ at the surface of the roughness elements, which do not necessarily align with the computational grid. The method has been extensively validated by the research group ensuring the correctness of the simulation results (see among others Leonardi et al. (2003), Orlandi and Leonardi (2006, 2008), Leonardi et al. (2007), Leonardi and Castro (2010)).

3. Flow configuration

Direct Numerical Simulations of a turbulence channel flow with roughness on the lower wall were performed (Fig. 1). Periodic boundary conditions were applied in the streamwise (x or x_1) and spanwise (z or x_3) directions, with a no-slip condition in the wall-normal direction (y or x_2). The computational domain is $6.4h \times 2.2h \times \pi h$ (the reference length scale h denotes the half-height of the channel measured from the crest plane of the roughness elements).

Two sets of simulations were carried out, varying the roughness height and keeping the pitch-to-height ratio fixed ($w/k = 4$). In the first set of simulations, 16 triangular transverse bars were placed on the bottom wall, with a constant roughness height of $k/h = 0.1$, as seen in the baseline case ($A1_1$), illustrated in Fig. 1a. In the second set, the number of bars was halved and the roughness height was doubled to $k/h = 0.2$ ($A1_2$), shown in Fig. 1b. Other cases involved modifications of the baseline, such as increasing the height of one element in cases $B1_1$ and $B1_2$, or removing the element immediately downstream of the tallest one in cases $B2_1$, $B2_2$, and $B2_{2b}$. Additionally, the set of simulations labeled with C included two taller triangles, with streamwise distances gradually increasing from $C1_1$ to $C4_1$ and from $C1_2$ to $C4_2$. The geometrical parameters and flow properties are summarized in Table 1. Based on the friction Reynolds number and k/h values, a fully rough regime was ensured, as discussed in Leonardi et al. (2007) and Bandyopadhyay (1987). The Reynolds number was set to $Re = 4,300$, resulting in a friction Reynolds number equal to $Re_\tau = 240$ for the smooth channel. For the rough surfaces, the drag increase and Re_τ ranged between 500 and 700. A grid of $512 \times 256 \times 256$ points was employed. A grid sensitivity study has been performed to check that the results did not depend on the resolution. The mesh is uniform in both the streamwise and spanwise directions, with spacings $\Delta x/h = 0.0125$ corresponding to $5 < \Delta x^+ < 9$ (depending on the particular roughness geometry) and $\Delta z/h = 0.009$, respectively. In the wall-normal direction, a non-uniform mesh was employed: the grid is refined near the wall and within the cavities, reaching a minimum spacing of $\Delta y_{\min}/h = 0.002$ (about 1 wall unit in inner scaling depending on the particular rough surface), and gradually coarsens toward the channel centerline, where the maximum spacing is $\Delta y_{\max}/h = 0.026$. Across all simulation sets, we ensured that the spanwise grid spacing in wall units, Δz^+, remained within the range 4–6 around the roughness elements. This range is in agreement with the values recommended in previous DNS studies performed in turbulent flows over rough surfaces (e.g., Chan et al. (2015), MacDonald et al. (2016)), which have demonstrated that such a resolution is sufficient to accurately capture the essential flow physics in the vicinity of roughness elements when using immersed boundary methods.

Particular attention has been given to resolving the sharp geometric features of the roughness elements, especially near the triangle peaks, where strong velocity gradients and intense vorticity can develop. These localized effects play a significant role in the formation of coherent structures that extend into the outer flow region. The relevance of such small-scale phenomena has been thoroughly discussed in Castro et al. (2021) and Castro and Wook (2024). To ensure adequate resolution of these effects, the base of each triangular element is covered by approximately 9 grid points in the configurations A, B, C with a subscript "1" and 17 grid points in the configurations A, B, C with a subscript "2". As previously discussed, in order to ensure a correct resolution of the small scales, a sensitivity analysis has been carried out by doubling the number of streamwise points from 512 to 1024. The results, not shown here, confirmed that the current grid resolution is sufficient to accurately capturing the relevant flow dynamics.

4. Results and discussion

The effect of roughness can be represented through the downward shift of the mean velocity U^+ profile, compared to that of a smooth wall, by the roughness function ΔU^+, expressed as:

$$U^+ = \kappa^{-1} \ln\ y^+ + C - \Delta U^+ \tag{4}$$

In this paper, the roughness function is determined as the offset of the log-region relative to an ideal smooth wall, with a constant value of $C = 5.6$. The friction velocity on the rough wall is computed as

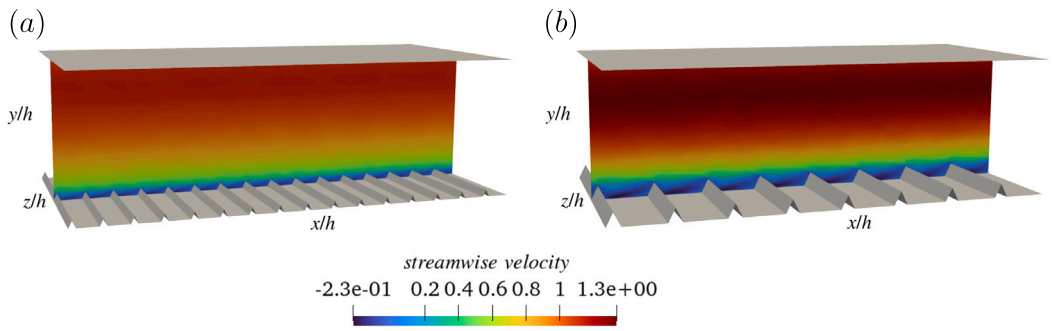

Fig. 1. Computational domain and color contours of streamwise averaged velocity: (a) $k/h = 0.1$; (b) $k/h = 0.2$.

Table 1
Geometrical and flow properties. k/h: roughness height; w/h: cavity width; ES: Effective Slope; ED: Effective Distribution; $D/\rho U_b^2$: total drag; ΔU^+: roughness function.

Marker	Case	k/h	w/h	ES	ED	$D/\rho U_b^2$	ΔU^+	Sketch
♦	Flat	0.00	0.00	0.00	0.00	0.12	0.30	
□	$A1_1$	0.10	0.40	0.50	0.57	0.23	11.50	
▲	$B1_1$	0.10	0.40	0.56	0.67	0.34	13.00	
▲	$B2_1$	0.10	0.40	0.50	0.69	0.35	13.00	
●	$C1_1$	0.09	0.40	0.56	0.66	0.28	12.20	
●	$C2_1$	0.09	0.40	0.56	0.69	0.31	12.80	
●	$C3_1$	0.09	0.40	0.56	0.71	0.37	13.50	
●	$C4_1$	0.09	0.40	0.56	0.73	0.38	13.80	
□	$A0$	0.20	6.40	0.06	0.25	0.23	11.00	
□	$A1_2$	0.20	0.80	0.50	0.65	0.35	13.50	
□	$A1_{2b}$	0.22	0.80	0.55	0.72	0.38	13.60	
▲	$B1_2$	0.20	0.80	0.56	0.77	0.52	14.60	
▲	$B2_2$	0.20	0.80	0.50	0.79	0.55	14.60	
▲	$B2_{2b}$	0.23	0.80	0.58	0.91	0.68	15.50	
●	$C1_2$	0.18	0.80	0.56	0.76	0.45	13.70	
●	$C2_2$	0.18	0.80	0.56	0.78	0.49	14.20	
●	$C3_2$	0.18	0.80	0.56	0.81	0.58	15.00	
●	$C4_2$	0.18	0.80	0.56	0.83	0.60	15.00	

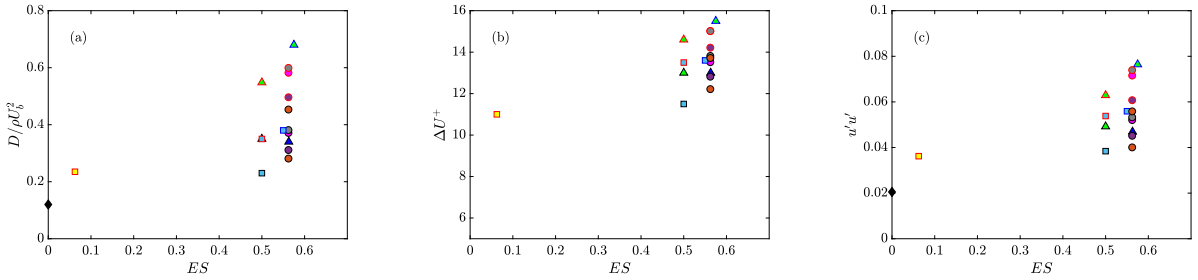

Fig. 2. Effective slope dependence on the Drag, roughness function and streamwise turbulent intensities of the rough wall.♦ Flat; □ $A1_1$; □ $A1_{1b}$; ▲ $B1_1$; ▲ $B2_1$; ● $C1_1$; ● $C2_1$; ● $C3_1$; ● $C4_1$; □ $A0$; □ $A1_2$; □ $A1_{2b}$; ▲ $B1_2$; ▲ $B2_2$; ▲ $B2_{2b}$, ● $C1_2$; ● $C2_2$; ● $C3_2$; ● $C4_2$. (For interpretation of the references to colour in this figure legend, the reader is referred to the web version of this article.)

the sum of form drag and frictional drag and further validated using the zero crossing of the Reynolds stress as in Leonardi et al. (2005), eliminating uncertainties arising from channel asymmetry. Once each wall is scaled with the appropriate friction velocity, the asymmetry of the geometrical configuration does not affect the results, as also discussed in several studies conducted using asymmetric channels (see, among others, Leonardi et al. (2003), Leonardi and Castro (2010), Flack and Schultz (2014), and references therein). In fact, velocity profiles on the upper smooth wall (not shown, as they are beyond this paper's scope) align well with the law of the wall when scaled using the proper friction velocity derived from shear on that wall (and not from the pressure drop). The extent of the log-region on the smooth wall is shorter due to the smaller local turbulent Reynolds number. The virtual origin in y is chosen such that the slope of the log-region corresponds to $\kappa = 0.41$. Although alternative choices for the virtual origin exist, fixing the slope to κ^{-1} ensures consistent roughness function calculations across analyzed cases.

One of the most recent challenges is to find a correlation between roughness parameter and the effect on turbulence (drag and ΔU^+). Among others, the Effective Slope ES, introduced by Napoli et al. (2008), ensured wide interest. Fig. 2 presents the total drag, roughness function and streamwise velocity variance as functions of Effective Slope ($ES = \frac{1}{L_{x_1}} \int_{L_{x_1}} \left| \frac{\partial k(x_1)}{\partial x_1} \right| dx_1$). For identical values of ES, the drag exhibits significant variations, up to 300%, while the roughness function varies by up to 40%. Similarly, the streamwise velocity variance varies significantly despite the same ES. Drag is included in the analysis because it is free from uncertainties associated with defining the roughness function, such as the choice of virtual origin, log-region

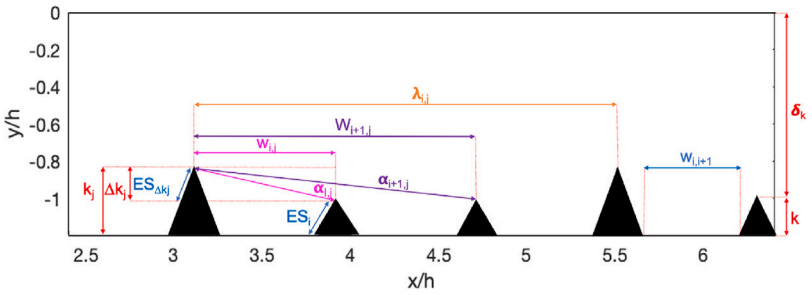

Fig. 3. Schematic representation of the parameter defined in the determination of the Effective Distribution (Bruno et al., 2024b).

slope, and constant C. It is worthwhile to notice how the roughness function values of the proposed geometries are quite high, starting from ΔU^+=11.0 up to 15.5. This is due to the specific geometry of the roughness composed by transverse 2D triangular bars. The results are in agreement with the findings of previous literature; see among others Leonardi et al. (2003), Ashrafian et al. (2004), Orlandi and Leonardi (2006), Schultz and Flack (2009).

Bruno et al. (2024b) analyzed the flow structure and pressure distribution around rough surfaces to understand why drag and roughness function can vary even when geometric statistics, such as mean roughness height, Effective Slope (ES), skewness, and kurtosis, remain constant. Their findings demonstrate that small changes in ES, such as the introduction of a single taller element, can significantly increase drag. For instance, a comparison between uniform triangular roughness surfaces $A1_1$ and $B1_1$, where $B1_1$ includes one taller element, revealed that this small change causes a significant rise in drag. This increase is attributed to flow streamlines impinging on the tallest element, resulting in form drag approximately eight times higher than in $A1_1$. In uniform roughness, flow recirculates within cavities, whereas the tallest pinnacles dominate the drag effects, a phenomenon not captured by ES. When an additional taller element is placed immediately downstream ($C1_1$), the mean surface height and moment statistics increase, yet drag and the roughness function decrease due to volumetric sheltering effects. However, when the distance between the tallest elements increases, as in $C3_1$ and $C4_1$, drag rises because the flow reattaches to lower elements, enhancing pressure drag. These results underscore the profound influence of roughness element position on drag and flow physics, even when geometric statistics remain constant. The presence of a single tall pinnacle exerts a disproportionate impact on drag, an effect amplified when upstream elements are shorter. To address these findings, Bruno et al. (2024b) introduced a revised parametrization, the Effective Distribution (ED), which extends the original ES framework introduced by Napoli et al. (2008):

$$\begin{cases} ED = (ES - ES_\alpha + ES_\beta) + \gamma \\ ES_\alpha = \sum_{j=1}^{m}\sum_{i=1}^{n} \alpha_{i,j} \cdot ES_i; \quad ES_\beta = \sum_{j=1}^{m}\sum_{i=1}^{m} \beta_{i,j} \cdot ES_{\Delta k_i}; \quad \gamma = \sum_{i=1}^{n} \frac{w_{i,i+1}}{L_x}\frac{k}{\delta_k} \\ \alpha_{i,j} = \min\left(1, \frac{\Delta k_j}{w_{i,j}}\right) \quad \text{for} \quad 1 \le \frac{w_{i,j}}{k} < 8, \quad \alpha_{i,j} = 0 \quad \text{for} \quad \frac{w_{i,j}}{k} > 8, \\ \beta_{i,j} = \frac{\lambda_{i,j}}{\text{wake}_j} \quad \text{for} \quad \frac{\lambda_{i,j}}{\text{wake}_j} < 1, \quad \beta_{i,j} = 1 \quad \text{for} \quad \frac{\lambda_{i,j}}{\text{wake}_j} > 1. \end{cases} \tag{5}$$

where ES is the overall Effective Slope calculated as in the original formulation of Napoli et al. (2008) ($\frac{1}{L_{x_1}}\int_{L_{x_1}}\left|\frac{\partial k(x_1)}{\partial x_1}\right| dx_1$), ES_i is the Effective Slope of the ith element, $w_{i,j}$ is the distance between the jth higher peak, emerging Δk_j over the crest plane, and the ith roughness element. The index n in the summations indicates the number of roughness elements while m is the number of pinnacles above the crests plane. Previous papers showed that for a pitch-to-height ratio larger than 8 the roughness elements act as isolated with a reattachment of the flow on the flat wall of the cavities, therefore the wake length can be approximated to $wake_j = 8k_j$. The ED accounts for the wake effects, element spacing, and roughness height gradients, providing a more comprehensive description of how geometry influences drag. Bruno et al. (2024b) highlights that the roughness elements located in the wake of larger elements contribute negligibly to drag. Consequently, the geometrical parameters used to describe roughness should account for the reduced influence of these elements within the wake length. The drag contribution of each roughness element is strongly influenced by its pattern and its distance from the upstream elements. Additionally, the spacing between consecutive roughness elements significantly impacts the velocity distribution, momentum within the cavity, and the intensity of the stagnation point on the windward side of the roughness element. In Fig. 3 a schematic representation of the parameter defined in Eq. (5) is depicted.

Fig. 4 highlights how each term contributes to the Effective Distribution differently, influencing the final roughness parametrization. Among these terms, the third term (pinnacles higher than the crest plane) and the fourth term (spacing between consecutive roughness elements) have the most significant impact on the final geometrical parameter, as shown in Fig. 4e. A similar trend is observed when plotting the correlations with the roughness function ΔU^+ (Fig. 5), confirming that the same roughness features, such as pinnacles and element spacing, play a crucial role in both drag and roughness function analyses.

Figs. 4f and 5f present the correlations between the Effective Distribution and both the total drag and the roughness function. The novel parametrization ED, proposed by Bruno et al. (2024b), correlates with the drag significantly better than the ES (shown in Fig. 2). A large variation in terms of drag, roughness function, and streamwise turbulent intensities for the same value of ES was observed in Fig. 2, suggesting that the Effective Slope alone may not fully capture the impact of geometrical features on turbulent flows. On the other hand, the Effective Distribution, taking into account the geometrical features that affect the turbulent flows discussed above, varies smoothly with both the drag and roughness function. Although the present study primarily focuses on idealized 2D triangular roughness to isolate the fluid dynamic behavior around individual elements, Bruno et al. (2024b) extended the analysis by using irregular 2D roughness, generated by the superposition of sinusoidal functions with random amplitudes and four different wavelengths, as studied in De Marchis et al. (2019). This approach produced a more complex topography, allowing for an investigation of how surface irregularities affect the mean flow, with particular emphasis on the role of crest elements. In Fig. 5f, the correlation between the data achieved by De Marchis et al. (2019) is presented, marked with the '$*$' symbol. Since the calculated ED value for this case was relatively low (0.15), Bruno et al. (2024b) performed a new simulation, resulting in an ED value of 0.37, while replicating the irregular surface analyzed by De Marchis et al. (2019). The point depicted in Fig. 5f using the $*$ marker follows the trend established for the regular triangular roughness examined here. These results suggest that the ED parameter can be generalized to different geometries, although further investigations are required to fully validate this claim.

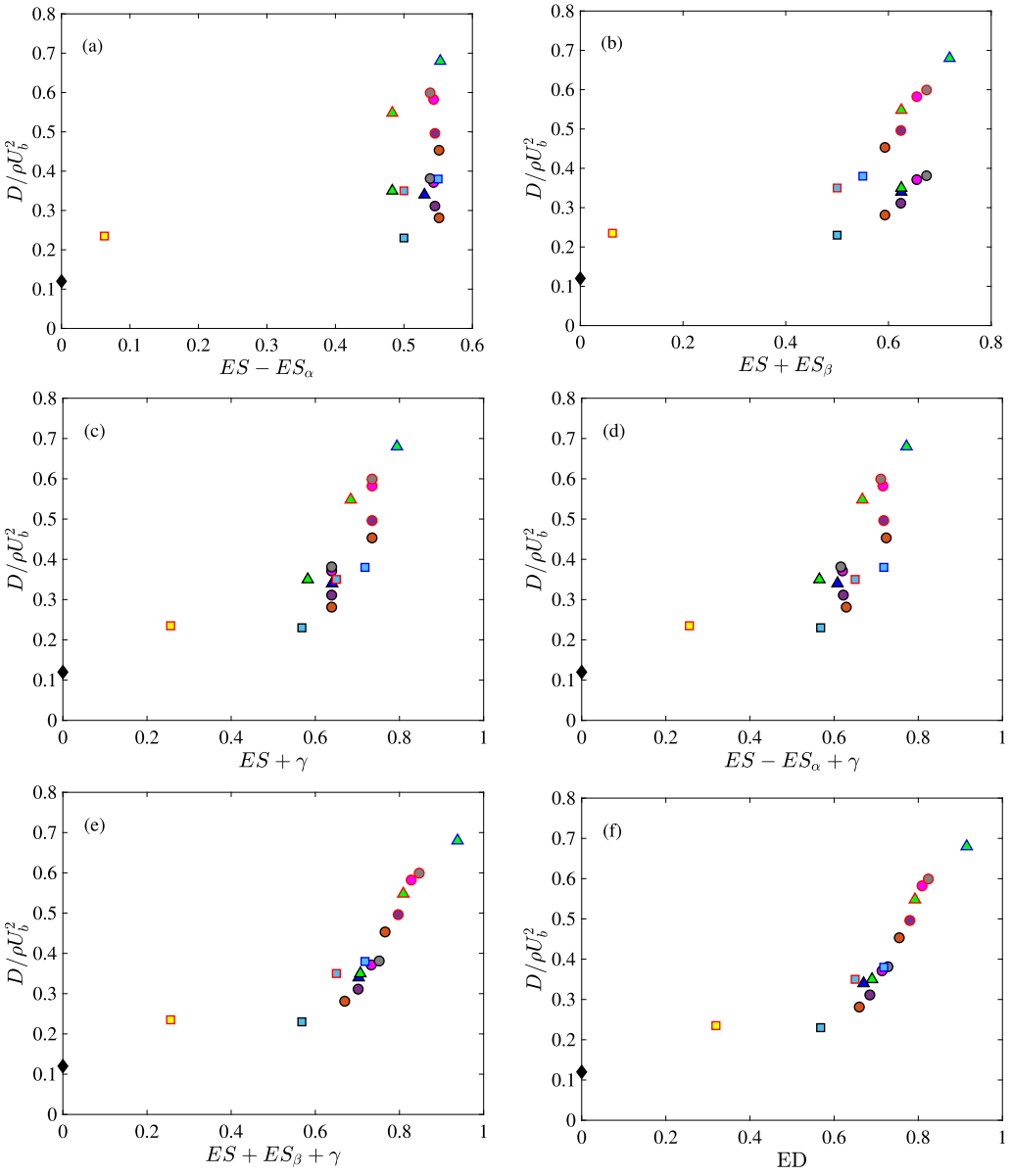

Fig. 4. Dependence of the drag on the terms of the effective distribution. Symbols as in Table 1. ♦ Flat; □ $A1_1$; □ $A1_{1b}$; ▲ $B1_1$; ▲ $B2_1$; ● $C1_1$; ● $C2_1$; ● $C3_1$; ● $C4_1$; □ $A0$; □ $A1_2$; □ $A1_{2b}$; ▲ $B1_2$; ▲ $B2_2$; ▲ $B2_{2b}$, ● $C1_2$; ● $C2_2$; ● $C3_2$; ● $C4_2$. (For interpretation of the references to colour in this figure legend, the reader is referred to the web version of this article.)

To illustrate how turbulence is influenced by the rough surfaces, a comparison of the turbulent intensities ($u'_{rms} = \sqrt{\langle u'u' \rangle}$, $v'_{rms} = \sqrt{\langle v'v' \rangle}$ and $w'_{rms} = \sqrt{\langle w'w' \rangle}$, where angular brackets denote averages in time, streamwise and spanwise direction) with respect to those in a smooth channel are shown in Figs. 6, 7, 8 and 9. Following some recent researches (see, among others Jelly and Busse (2018)) the intrinsic spatial-average was used, thus ensuring that only the regions, between the roughness, occupied by fluids, are considered. The other type of average, the so-called superficial average, takes into account all the domain volume, occupied by the solid boundary and by the fluid; recently, the properties of intrinsic and superficial averages and their effect on mean profiles with example data were illustrated by Schmid et al. (2019). There are no differences among the two types of averages above the roughness layer.

The increased drag over the rough walls, observed in Fig. 4, corresponds to higher turbulent intensities when scaled with external units. Roughness-induced disturbances lead to significant changes in stresses near the crest plane and the outer region, which are driven by events occurring in the near-wall region. For all rough surfaces, the wall-normal turbulent intensity profile remains constant near the roughness and reaches a maximum at the crest plane as observed in Figs. 6c–d and in Figs. 7c–d. The maximum value of turbulent intensities depends on the geometrical shape, with the largest values observed for $C4_1$ and $C4_2$ (the cases with two pinnacles more spaced with respect to the other cases). The turbulent intensities (consistently with the drag) increase with the size of the roughness from $k/h = 0.1$ to $k/h = 0.2$.

A different trend emerges when the root-mean-square (rms) values on the rough wall side are scaled with the local friction velocity u_τ, as plotted in Fig. 8 and in Fig. 9. In agreement with previous contributions, see among others Bhaganagar et al. (2004) and Orlandi and Leonardi (2006), Figs. 8 and 9 show a reduction in the near-wall maxima of u^+_{rms} (a + indicates scaling in inner units) and an increase of v^+_{rms} and v^+_{rms} (although not as large as observed when scaled in external units). This is because while on a smooth wall, the friction is due to the shear which is well correlated with the velocity fluctuations, over a rough wall, the drag and then the friction velocity is partially

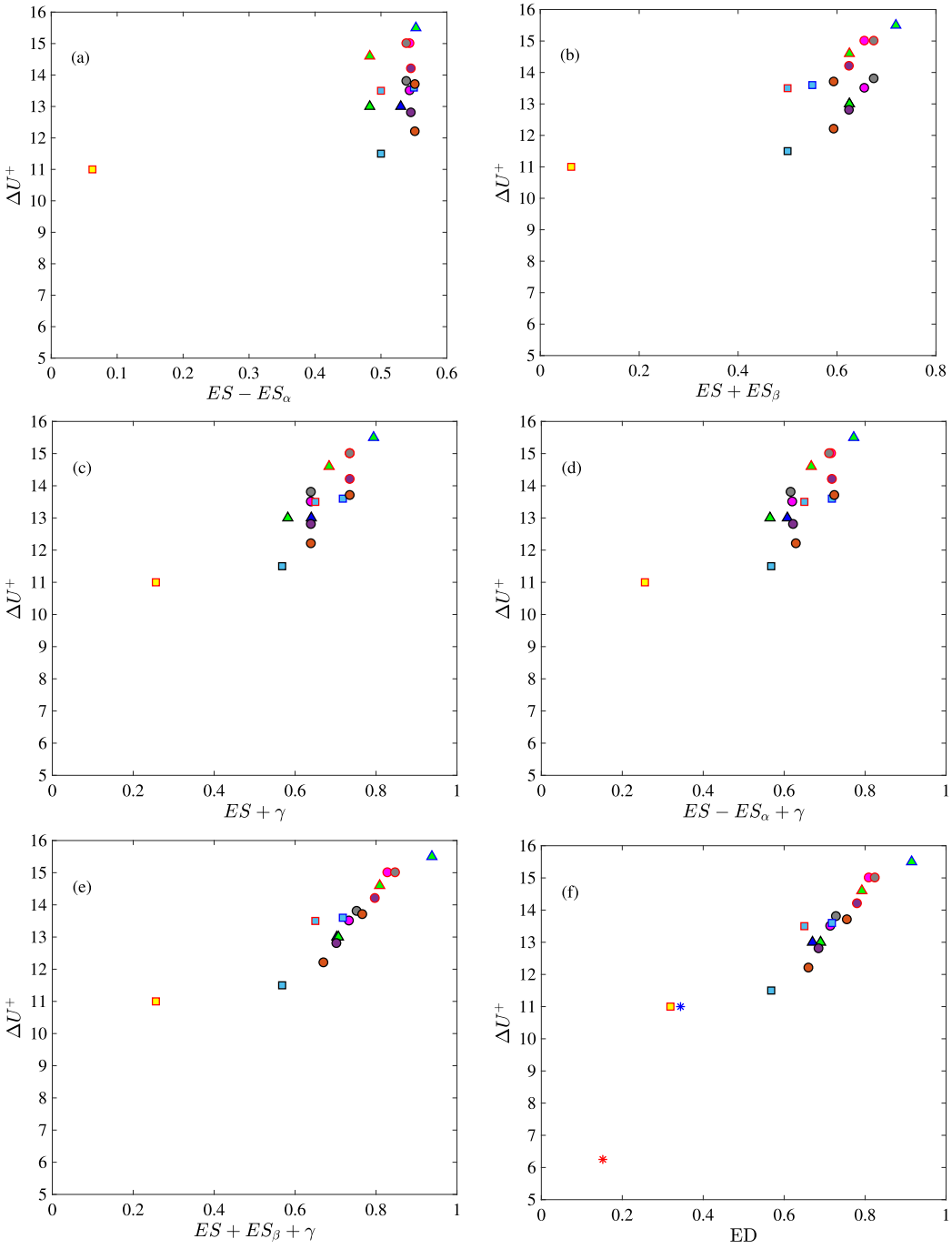

Fig. 5. Terms of the Effective Distribution dependence on the roughness function. ♦ Flat; □ $A1_1$; □ $A1_{1b}$; ▲ $B1_1$; ▲ $B2_1$; ● $C1_1$; ● $C2_1$; ● $C3_1$; ● $C4_1$; □ $A0$; □ $A1_2$; □ $A1_{2b}$; ▲ $B1_2$; ▲ $B2_2$; ▲ $B2_{2b}$, ● $C1_2$; ● $C2_2$; ● $C3_2$; ● $C4_2$; ∗ De Marchis et al. (2019); ∗ crest roughness type. (For interpretation of the references to colour in this figure legend, the reader is referred to the web version of this article.)

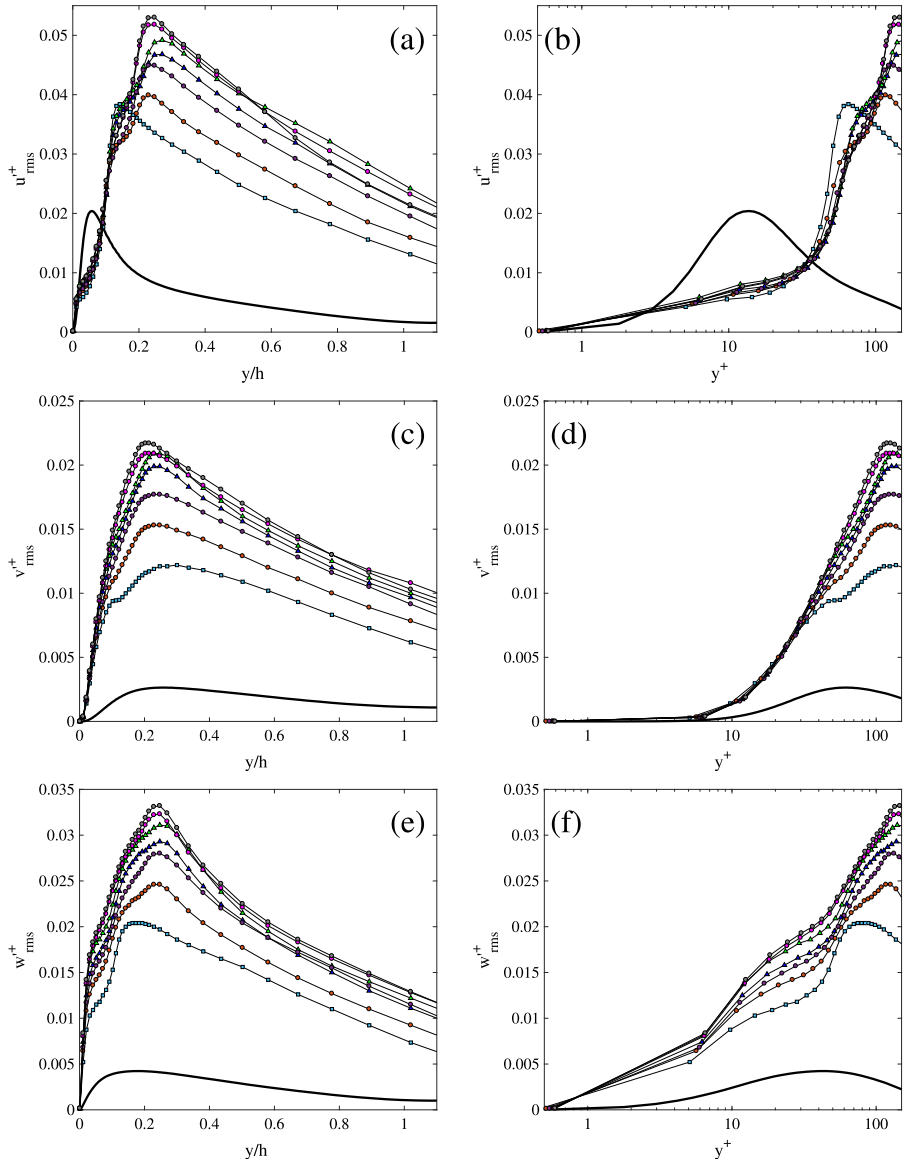

Fig. 6. Turbulent intensities in external units for $k/h = 0.1$. (a)–(b): streamwise component u'_{rms}; (c)–(d): wall-normal component v'_{rms}; (e)–(f): spanwise component w'_{rms}. ♦ Flat; $A1_1$; $A1_{1b}$; $B1_1$; $B2_1$; $C1_1$; $C2_1$; $C3_1$; $C4_1$; $A0$; $A1_2$; $A1_{2b}$; $B1_2$; $B2_2$; $B2_{2b}$, $C1_2$; $C2_2$; $C3_2$; $C4_2$. (For interpretation of the references to colour in this figure legend, the reader is referred to the web version of this article.)

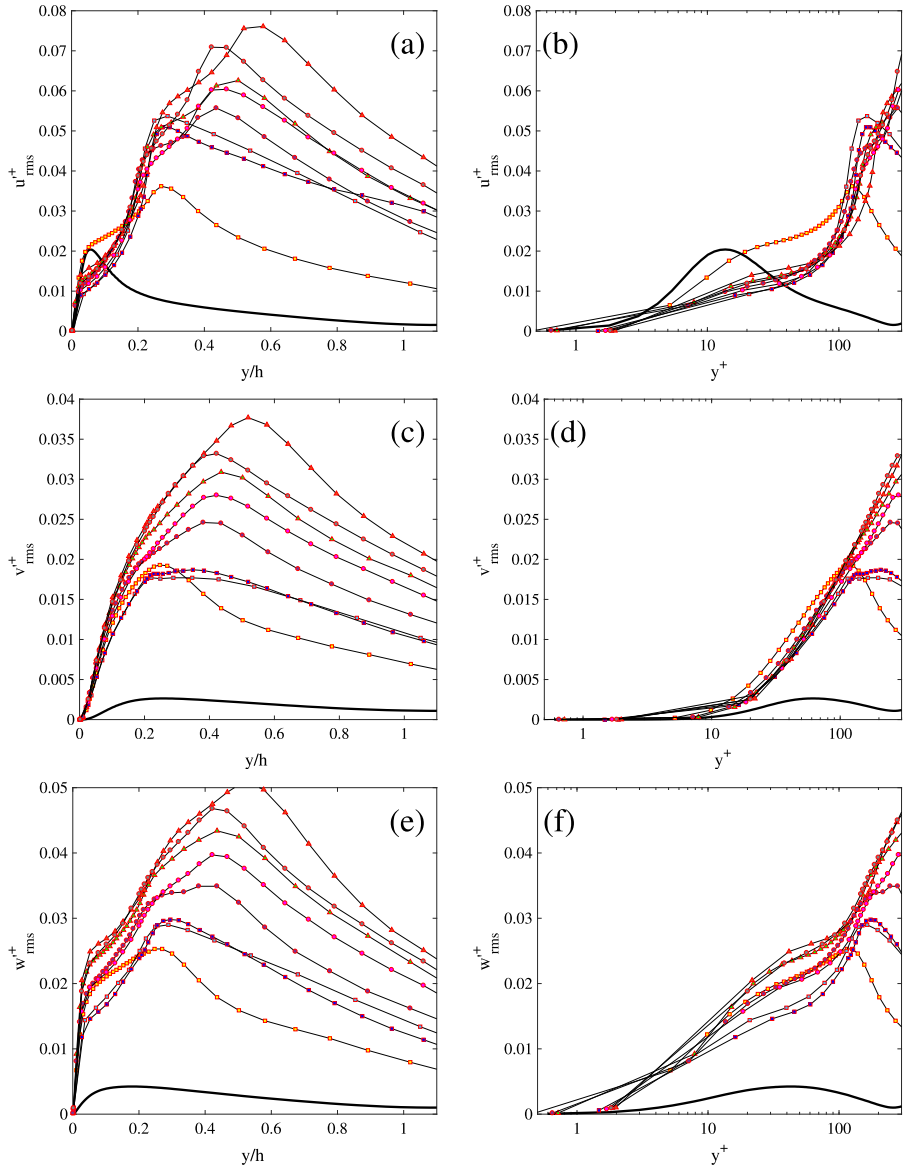

Fig. 7. Turbulent intensities in external units for $k/h = 0.2$. (a)–(b): streamwise component u'_{rms}; (c)–(d): wall-normal component v'_{rms}; (i)–(n): spanwise component w'_{rms}. ♦ Flat; $A1_1$; $A1_{1b}$; $B1_1$; $B2_1$; $C1_1$; $C2_1$; $C3_1$; $C4_1$; $A0$; $A1_2$; $A1_{2b}$; $B1_2$; $B2_2$; $B2_{2b}$, $C1_2$; $C2_2$; $C3_2$; $C4_2$. (For interpretation of the references to colour in this figure legend, the reader is referred to the web version of this article.)

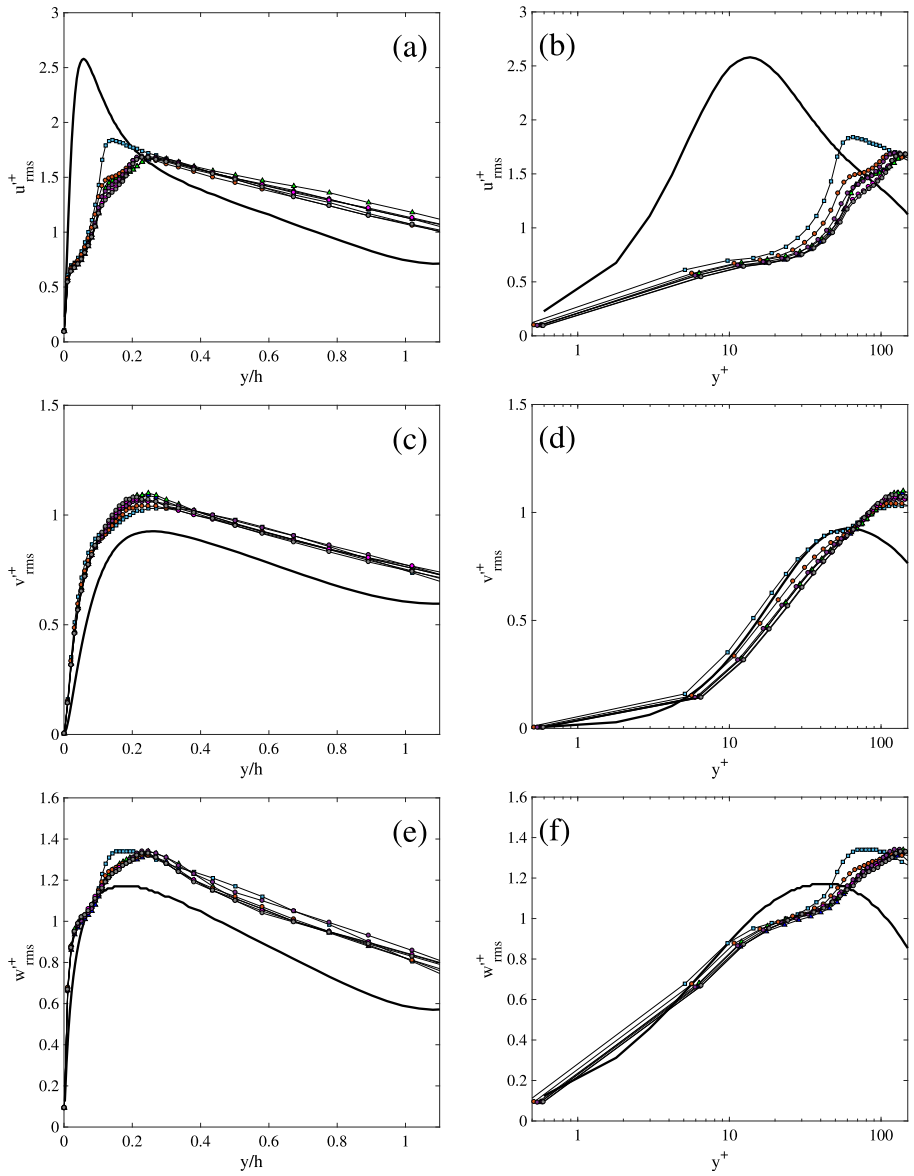

Fig. 8. Turbulent intensities in wall units for $k/h = 0.1$. (a)–(b): streamwise component u^+_{rms}; (c)–(d): wall-normal component v^+_{rms}; (e)–(f): spanwise component w^+_{rms}. ♦ Flat; □ $A1_1$; □ $A1_{1b}$; ▲ $B1_1$; ▲ $B2_1$; ● $C1_1$; ● $C2_1$; ● $C3_1$; ● $C4_1$; □ $A0$; □ $A1_2$; □ $A1_{2b}$; ▲ $B1_2$; ▲ $B2_2$; ▲ $B2_{2b}$, ● $C1_2$; ● $C2_2$; ● $C3_2$; ● $C4_2$. (For interpretation of the references to colour in this figure legend, the reader is referred to the web version of this article.)

due to the pressure drag. Over a rough wall, both the friction velocity and the velocity fluctuations increase with respect to a smooth wall. The larger is the form drag, the more the friction velocity increases with respect to the velocity fluctuations resulting in the trend shown in Figs. 9–10. The position of the peak is shifted with respect to the smooth wall. If the vertical origin is taken on the bottom wall, the position of the maxima are shifted upward. The opposite is observed if the origin is taken at the crests plane. Similarly, shifting the vertical origin the fluctuations on the outer region can overlap those relative to a smooth wall. Parameterizing the drag provides valuable insights into momentum loss, turbulence, and mixing induced by roughness. However, despite efforts to correlate data with mean roughness height or rms, significant scatter persists, underscoring the complexity of capturing roughness effects on drag and turbulence with high precision. The color contour of streamwise turbulent intensities for select cases is shown in Fig. 10. When comparing $A1_1$ (Fig. 10a □, uniform triangles) and $B1_1$ (Fig. 10b ▲, the same as $A1_1$ but with a higher pinnacle element, Δk), it is evident that the introduction of a taller pinnacle leads to a significant increase in u'_{rms}. For the uniform roughness case ($A1_1$), turbulent intensities remain relatively uniform within the roughness sublayer, without notable peaks near individual elements. In contrast, $B1_1$ exhibits a localized peak in u'_{rms}, driven by strong velocity gradients and enhanced turbulence near the stagnation point on the windward side of the tallest element, extending downstream into the wake. This increase in u'_{rms} in $B1_1$ suggests higher turbulent mixing and greater energy fluctuations compared to the uniform triangular roughness in $A1_1$. Similar observations can be made comparing $A1_2$ and $B1_2$ (Figs. 10c and d), where the taller pinnacle further amplifies turbulence and mixing. Furthermore, the rms of flow fluctuations behind the pinnacles is notably low, and within the wake, it approaches zero, indicating that the surface perturbations have a localized effect on the flow, with the most significant influence observed downstream in the wake region. Comparing Figs. 10a and 10c, as well as Figs. 10b and 10d, a general increase in u'_{rms} is observed as the roughness height increases from $k/h = 0.1$ to $k/h = 0.2$. This trend aligns with previous studies indicating that both drag and turbulent intensities are positively correlated with roughness height, highlighting that larger roughness elements promote stronger turbulence and higher momentum losses.

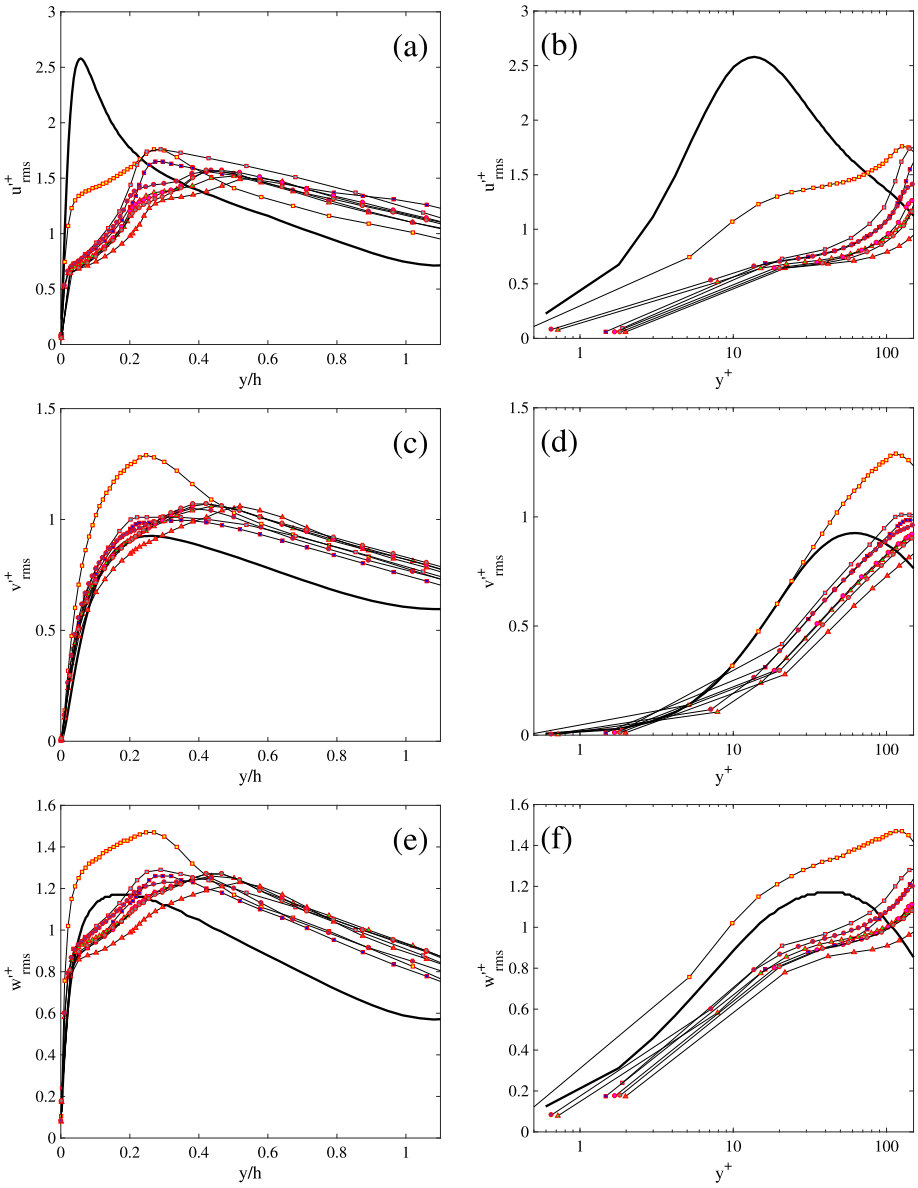

Fig. 9. Turbulent intensities in wall units for $k/h = 0.2$. (a)–(b): u^+_{rms}; (c)–(d): wall-normal component v^+_{rms}; (e)–(f): spanwise component w^+_{rms}. ♦ Flat; $A1_1$; $A1_{1b}$; $B1_1$; $B2_1$; $C1_1$; $C2_1$; $C3_1$; $C4_1$; $A0$; $A1_2$; $A1_{2b}$; $B1_2$; $B2_2$; $B2_{2b}$, $C1_2$; $C2_2$; $C3_2$; $C4_2$. (For interpretation of the references to colour in this figure legend, the reader is referred to the web version of this article.)

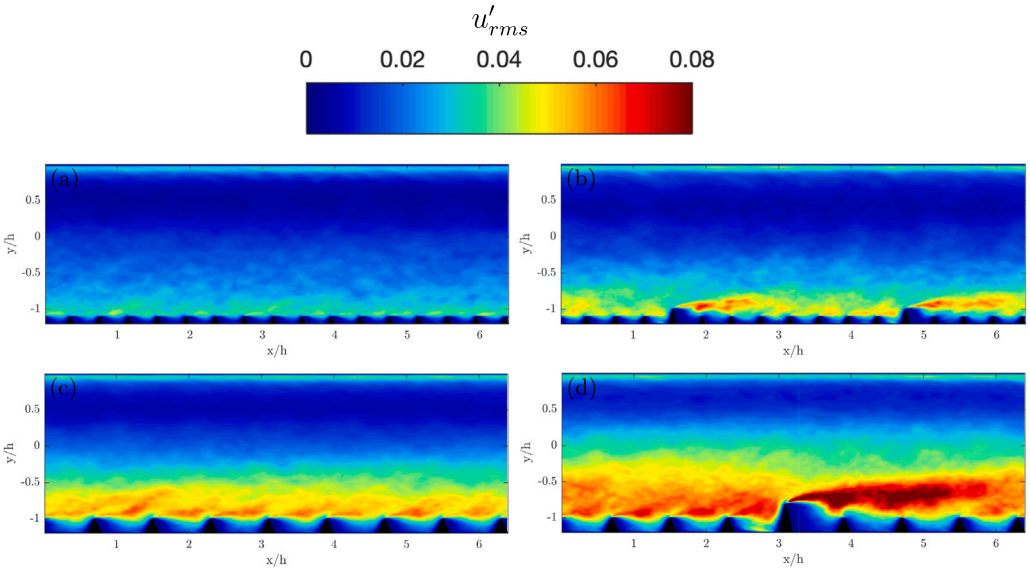

Fig. 10. Color contours of streamwise velocity turbulent intensities: (a) $A1_1$ (□), (b) $B1_1$ (▲), (c) $A1_2$ (□), (d) $B1_2$ (▲). (For interpretation of the references to colour in this figure legend, the reader is referred to the web version of this article.)

5. Conclusions

Building on the findings of Bruno et al. (2024b), Direct Numerical Simulations performed to analyze a set of 2D rough surfaces using triangle-shaped elements have been extended by incorporating an examination of turbulent intensities. The ED consistently incorporates the influence of flow dynamics around roughness elements, including wake effects and interactions between peaks, providing a more comprehensive representation of the roughness configuration. The Effective Distribution thus offers an improved correlation with both drag and roughness function over a wide range of surface configurations, including more realistic irregular rough surfaces generated using random sinusoidal functions. A detailed analysis of the terms of the ED equation has revealed the contributions of each roughness element. In fact, by isolating individual terms of the ED, a deeper insight into how different surface features influence turbulence has been provided. Specifically, the dominant role of the highest pinnacles and of the spacing between roughness elements has been found. On the other hand, the sheltering effect plays a fundamental role when a small triangle is quite close to an highest pinnacle. To further investigate on this behavior the turbulent intensities have been investigated. The analysis of rms values has demonstrated that the tallest roughness elements contribute to an huge increase in turbulent fluctuations. Despite the strong correlations observed, further work is necessary to extend the applicability of the ED to more complex rough surface configurations, particularly those exhibiting irregularities in the spanwise direction.

CRediT authorship contribution statement

Federica Bruno: Writing – original draft, Visualization, Validation, Supervision, Software, Resources, Methodology, Investigation, Funding acquisition, Formal analysis, Data curation, Conceptualization. **Mauro De Marchis:** Writing – original draft, Visualization, Validation, Supervision, Resources, Methodology, Investigation, Funding acquisition, Formal analysis, Data curation, Conceptualization. **Stefano Leonardi:** Writing – original draft, Visualization, Validation, Supervision, Software, Resources, Methodology, Investigation, Funding acquisition, Formal analysis, Data curation, Conceptualization.

Declaration of competing interest

The authors declare that they have no known competing financial interests or personal relationships that could have appeared to influence the work reported in this paper.

Acknowledgments

The authors greatly appreciate the financial support provided by the following projects:

- SL and FB were partially supported by National Science Foundation, United States grant n. 2202710;
- RETURN Extended Partnership and received funding from the European Union Next-GenerationEU (National Recovery and Resilience Plan – NRRP, Mission 4, Component 2, Investment 1.3 – D.D. 1243 2/8/2022, E0000005);
- The Texas Advanced Computing Center, and High Performance Computing at UT Dallas are acknowledged for providing computational time.
- TiSento - SENSORIALIZED COMPOSITE PIPE FOR HYDRAULIC APPLICATIONS, n. 084221000550 CUP G18I18001710007. Funded under measure 1.1.5 of the PO FESR SICILY 2014–2020;
- This research has been partially supported by the European Union - NextGenerationEU - National Sustainable Mobility Center CN00000023, Italian Ministry of University and Research Decree n. 1033— 17/06/2022, Spoke 3, CUP B73C22000760001

Data availability

Data will be made available on request.

References

Ashrafian, A., Andersson, H.I., Manhart, M., 2004. DNS of turbulent flow in a rod-roughened channel. Int. J. Heat Fluid Flow 25 (3), 373–383.

Bandyopadhyay, P.R., 1987. Rough-wall turbulent boundary layers in the transition regime. J. Fluid Mech. 180, 231–266. http://dx.doi.org/10.1017/S0022112087001794.

Bhaganagar, K., Kim, J., Coleman, G., 2004. Effect of roughness on wall-bounded turbulence. Flow Turbul. Combust. 72, 463–492.
Bons, J., 2005. A critical assessment of Reynolds analogy for turbine flows. J. Heat Transf. 127 (5), 472–485.
Bruno, F., De Marchis, M., Napoli, E., 2024a. The role of the areal parameters on turbulent flow over 2D Gaussian roughness. Int. J. Heat Fluid Flow 106, 109287.
Bruno, F., Leonardi, S., De Marchis, M., 2024b. Towards a new roughness parametrization through the effective distribution function. J. Fluid Mech. 999, A26.
Busse, A., Thakkar, M., Sandham, N.D., 2017. Reynolds-number dependence of the near-wall flow over irregular rough surfaces. J. Fluid Mech. 810, 196–224.
Castro, I.P., Kim2, J., Stroh, A., Lim, H., 2021. Channel flow with large longitudinal ribs. J. Fluid Mech. 915, A92.
Castro, I.P., Wook, K.J., 2024. Secondary motions in turbulent ribbed channel flows. J. Fluid Mech. 988, A2.
Chan, L., MacDonald, M., Chung, D., Hutchins, N., Ooi, A., 2015. A systematic investigation of roughness height and wavelength in turbulent pipe flow in the transitionally rough regime. J. Fluid Mech. 771, 743–777.
Chung, D., Hutchins, N., Schultz, M.P., Flack, K.A., 2021. Predicting the drag of rough surfaces. Annu. Rev. Fluid Mech. 53, 439–471.
De Marchis, M., Milici, B., Napoli, E., 2017. Solid sediment transport in turbulent channel flow over irregular rough boundaries. Int. J. Heat Fluid Flow 65, 114-126.
De Marchis, M., Milici, B., Napoli, E., 2019. Large eddy simulations on the effect of the irregular roughness shape on turbulent channel flows. Int. J. Heat Fluid Flow 80, 108494.
De Marchis, M., Saccone, D., Milici, B., Napoli, E., 2020. Large eddy simulations of rough turbulent channel flows bounded by irregular roughness: Advances toward a universal roughness correlation. Flow Turbul. Combust. 105 (2), 627–648.
Flack, K.A., Schultz, M.P., 2010. Review of hydraulic roughness scales in the fully rough regime. J. Fluids Eng. 132 (4).
Flack, K.A., Schultz, M.P., 2014. Roughness effects on wall-bounded turbulent flows. Phys. Fluids 26 (10).
Flack, K.A., Schultz, M.P., Volino, R.J., 2020. The effect of a systematic change in surface roughness skewness on turbulence and drag. Int. J. Heat Fluid Flow 85, 108669.
Forooghi, P., Stroh, A., Magagnato, F., Jakirlić, S., Frohnapfel, B., 2017. Toward a universal roughness correlation. J. Fluids Eng. 139 (12).
Hama, F.R., 1954. Boundary layer characteristics for smooth and rough surfaces. Trans. Soc. Nav. Arch. Mar. Engrs. 62, 333–358.
Jelly, T.O., Busse, A., 2018. Reynolds and dispersive shear stress contributions above highly skewed roughness. J. Fluid Mech. 852, 710–724.
Jiménez, J., 2004. Turbulent flows over rough walls. Annu. Rev. Fluid Mech. 36, 173–196.
Leonardi, S., Castro, I.P., 2010. Channel flow over large cube roughness: a direct numerical simulation study. J. Fluid Mech. 651, 519–539.
Leonardi, S., Orlandi, P., Antonia, R.A., 2005. A method for determining the frictional velocity in a turbulent channel flow with roughness on the bottom wall. Exp. Fluids 38, 796–800.
Leonardi, S., Orlandi, P., Antonia, R.A., 2007. Properties of d- and k-type roughness in a turbulent channel flow. Phys. Fluids 19 (125101).
Leonardi, S., Orlandi, P., Smalley, R., Djenidi, L., Antonia, R., 2003. Direct numerical simulations of turbulent channel flow with transverse square bars on one wall. J. Fluid Mech. 491, 229–238.
MacDonald, M., Chan, L., Chung, D., Hutchins, N., Ooi, A., 2016. Turbulent flow over transitionally rough surfaces with varying roughness densities. J. Fluid Mech. 804, 130–161.
Napoli, E., Armenio, V., De Marchis, M., 2008. The effect of the slope of irregularly distributed roughness elements on turbulent wall-bounded flows. J. Fluid Mech. 613, 385–394.
Nikuradse, J., 1933. Laws of flow in rough pipes. NACA TM 1292 (1950). National Advisory Commission for Aeronautics, pp. 1–62.
Oke, T.R., 1988. Street design and urban canopy layer climate. Energy Build. 11 (1–3), 103–113.
Orlandi, P., Leonardi, S., 2006. DNS of turbulent channel flows with two-and three-dimensional roughness. J. Turbul. (7), N73.
Orlandi, P., Leonardi, S., 2008. Direct numerical simulation of three-dimensional turbulent rough channels: parameterization and flow physics. J. Fluid Mech. 606, 399–415.
Piomelli, U., 2019. Recent advances in the numerical simulation of rough-wall boundary layers. Phys. Chem. Earth Parts A/B/C 113, 63–72.
Schlichting, H., 1937. Experimental Investigation of Surface Roughness. Technical Memorandum, (TM 823), NACA.
Schmid, M.F., Lawrence, G.A., Parlange, M.B., Giometto, M.G., 2019. Volume averaging for urban canopies. Bound.-Layer Meteorol. 173 (3), 349–372.
Schultz, M.P., Flack, K.A., 2009. Turbulent boundary layers on a systematically varied rough wall. Phys. Fluids 21 (1).
Sigal, A., Danberg, J.E., 1990. New correlation of roughness density effect on the turbulent boundary layer. AIAA J. 28 (3), 554–556.
Thakkar, M., Busse, A., Sandham, N., 2017. Surface correlations of hydrodynamic drag for transitionally rough engineering surfaces. J. Turbul. 18 (2), 138–169.
Van Rij, J.A., Belnap, B., Ligrani, P., 2002. Analysis and experiments on three-dimensional, irregular surface roughness. J. Fluids Eng. 124 (3), 671–677.
Waigh, D., Kind, R., 1998. Improved aerodynamic characterization of regular three-dimensional roughness. AIAA J. 36 (6), 1117–1119.